Supplementary Information

A NiFe-based monolithic electrocatalyst for pleiotropic-efficiency water oxidation

Yuting Li [a], Weihua Ma [a], Juan Wang [*a], Qin Zhong [*a]

[a] School of Chemistry and Chemical Engineering, Nanjing University of Science and Technology, Nanjing, Jiangsu, 210094, China.

*Corresponding author

E-mail: wangjuan304@njust.edu.cn, zq304@njust.edu.cn

Experimental Detail

Materials

Polyacrylonitrile (PAN, Mg: 48,000) was supplied by Sinopec Shanghai Petrochemical (shanghai, China). Thiourea, N, N-dimethylformamide (DMF) and $Fe(NO_3)_3 \cdot 9H_2O$, $Ni(NO_3)_2 \cdot 6H_2O$ were purchased from Shanghai Chemical Reagents. All chemicals were used directly without further purification.

Characterization

The scanning electron microscopy (SEM) characterization was recorded on a FEI Quanta 250FEG. The high-resolution transmission electron microscopy (HRTEM) and elemental mapping analysis were collected via a Tecnai G2F30 S-Twin. X-ray power diffraction (XRD) pattern was obtained with a Cu Kα radiation on a Bruker D8 ADVANCE diffractometer (λ = 1.5604 Å). The Raman spectra was performed on Aramis confocal Raman microscope (λ = 532 nm). X-ray photoelectron spectroscopy (XPS) was tested on a Thermo-VG Scientific Escalab 250Xi spectrometer with Al Kα X-ray source. The nitrogen adsorption-desorption characterization was investigated with an ASAP2460

Micromeritics equipment at 77 K. *In situ* FTIR spectra was tested on Thermo Scientific Nicolet iZ10. ICP analysis was detected on Perkinelmer Avio 500.

Electrochemical measurements

All potentials were referenced to the reversible hydrogen electrode (RHE) according to the equation: $E_{RHE} = E_{Hg/HgO} + 0.059 \times pH + 0.098\,V$. Linear sweep voltammetry (LSV) was carried out at a scan rate of 2 mV s^{-1}. Electrochemical impedance spectroscopy (EIS) was measured at 0.17 V with frequency ranging from 10^5 Hz to 1 Hz at an AC amplitude of 5 mV. The stability performance was measured by the chronopotentiometry method at a constant voltage of 1.5 V vs RHE.

The catalyst's electrochemically active surface area (ECSA) was evaluated by measuring the double-layer capacitance (C_{dl}) with cyclic voltammetry. The ECSA was obtained according to the following equation:

$$ECSA = \frac{C_{dl}}{C_S}$$

where C_s is the specific capacitance of atomically smooth planar per unit area with the value of 40 μF·cm^{-2} in alkaline electrolyte.[1]

The following formula was used to calculate the turnover frequency (TOF) values:

$$TOF = \frac{I}{4FM}$$

where I is the current at a specific overpotential; 4 is the electron transfer number for OER; F is the Faradic constant (96,485 C·mol^{-1}); M is the number of active sites (mol), which can be determined according to previous study reported by Yan et al.[2]

The faradaic efficiency (FE) for OER was studied by rotating ring-disk electrode (RRDE). The generated O_2 molecules were detected by oxygen reduction reaction when the ring potential was 0.4 V. The FE value of O_2 was calculated using the following equation:[1]

$$FE = \frac{I_{ring}}{I_{disk} \times N}$$

Where I_{ring} means the ring current. I_{disk} denotes the disk current. N represents the collection efficiency (here is 0.2).

In situ Raman measurement

The *in situ* Raman spectra was collected on a Raman microscope (LabRAM HR evolution, HORIBA) excited with a 532 nm laser and a power of 1 mW. The prepared catalyst (working electrode), graphene rod (counter electrode), and Hg/HgO (reference electrode) are inserted into a custom-made spectral-electrochemical cell filled with 1 M KOH electrolyte, which is displayed in Fig. S11. The as-prepared fibrous catalyst was directly clamped as a working electrode. Before carrying out the *in situ* Raman experiments, the sample had been activated via multiple CV scans for 5-6 h under scan rate of 2 mV s^{-1}. Each Raman spectra was collected with an acquisition time of 20 s under current-time (i-t) measurement at a constant potential by a confocal Raman microscope coupled with 50×objective.

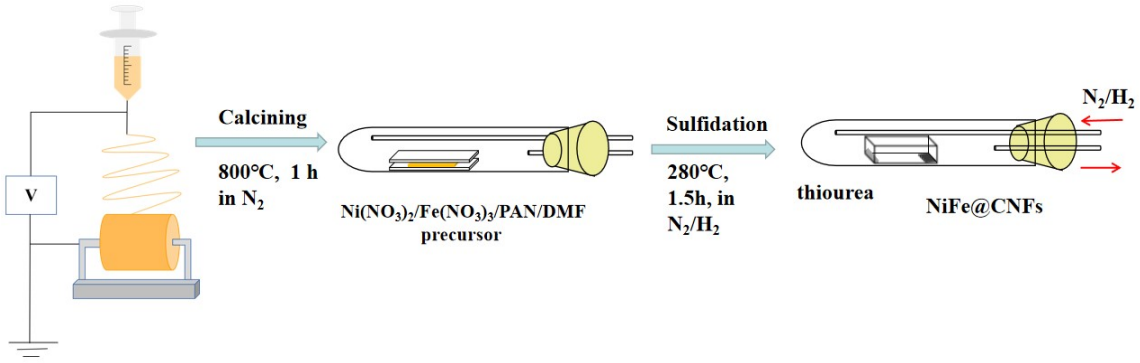

Fig. S1 Illustration of the synthetic process for NiFe-S@CNFs.

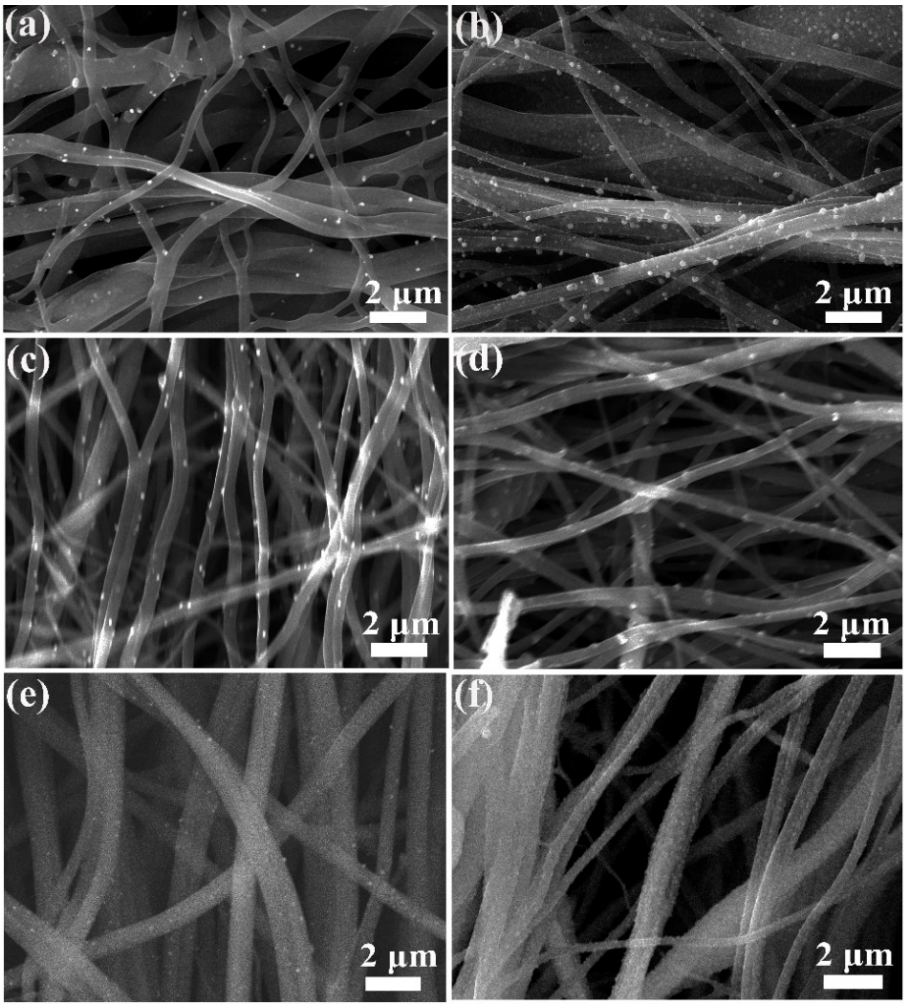

Fig. S2 SEM images of (a) Ni@CNFs, (b) Ni_3S_2@CNFs, (c) NiFe-31@CNFs, (d) NiFe-S-31@CNFs, (e) NiFe-11@CNFs and (f) NiFe-S-11@CNFs.

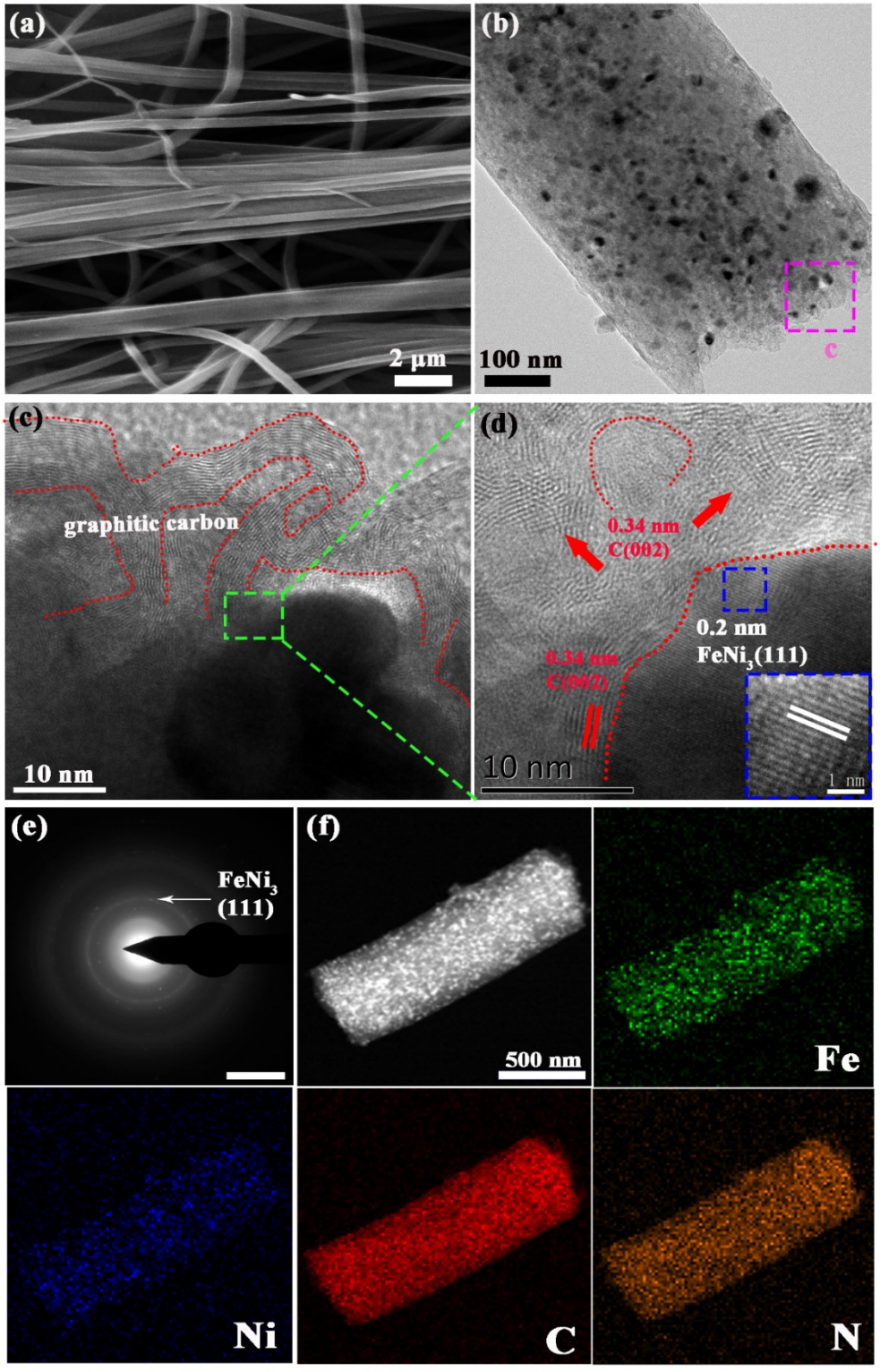

Fig. S3 (a) SEM image of the NiFe-13@CNFs; (b) TEM and (c, d) High-resolution TEM images of NiFe-13@CNFs; (e) corresponding SAED pattern of NiFe-13@CNFs; (f) Element mapping images of NiFe-13@CNFs.

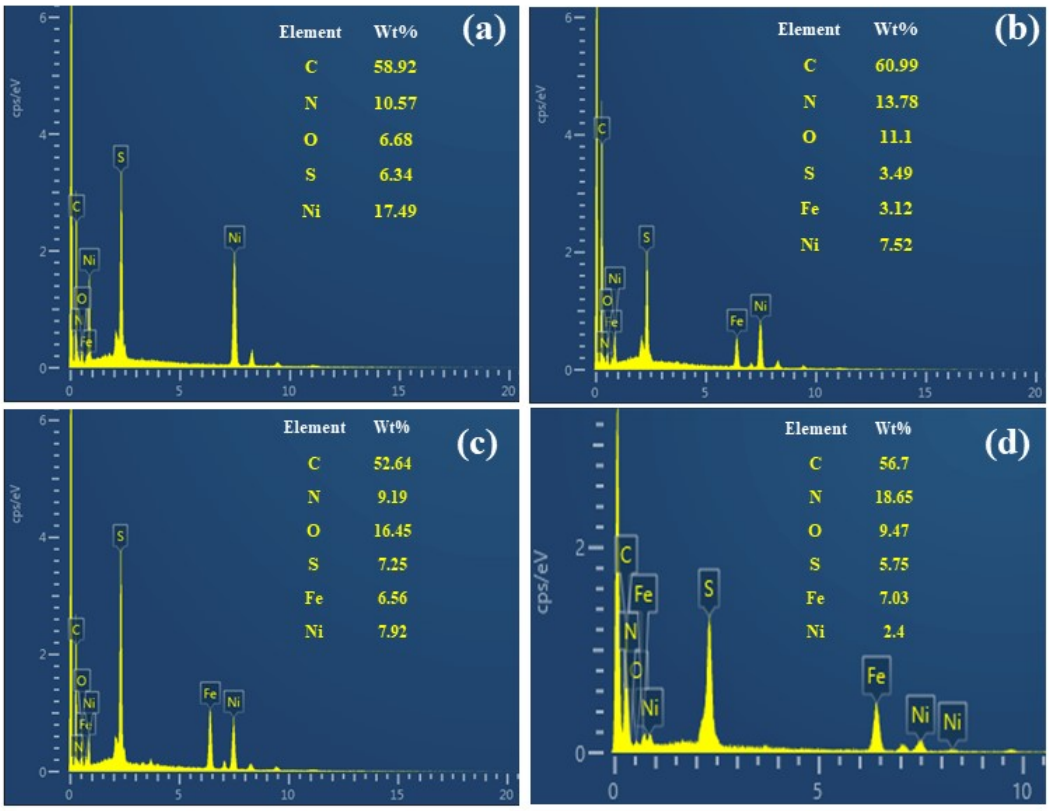

Fig. S4 EDX spectra and corresponding element contents of (a) Ni_3S_2@CNFs, (b) NiFe-S-31@CNFs, (c) NiFe-S-11@CNFs and (d) NiFe-S-13@CNFs samples.

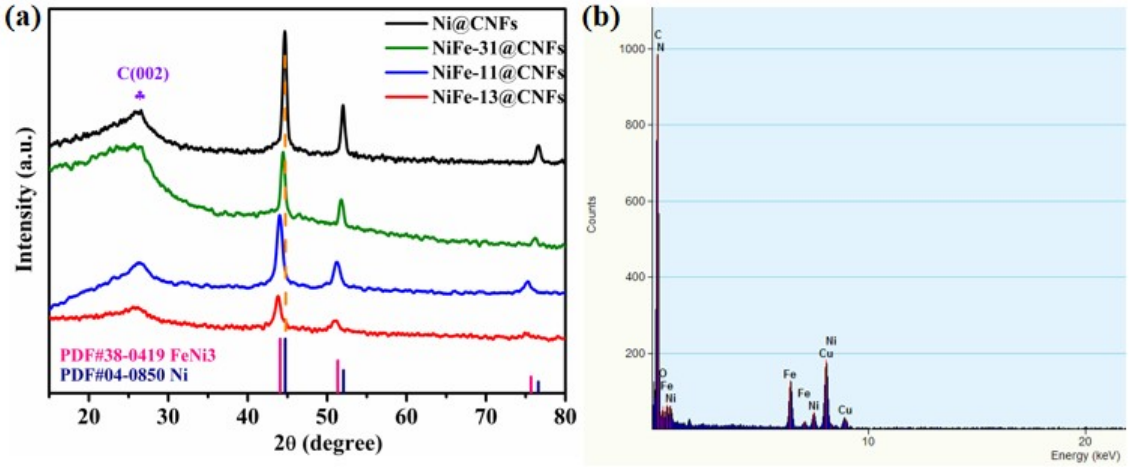

Fig. S5 (a) XRD patterns of alloy NiFe-xy@CNFs; (b) EDX spectra of NiFe-13@CNFs.

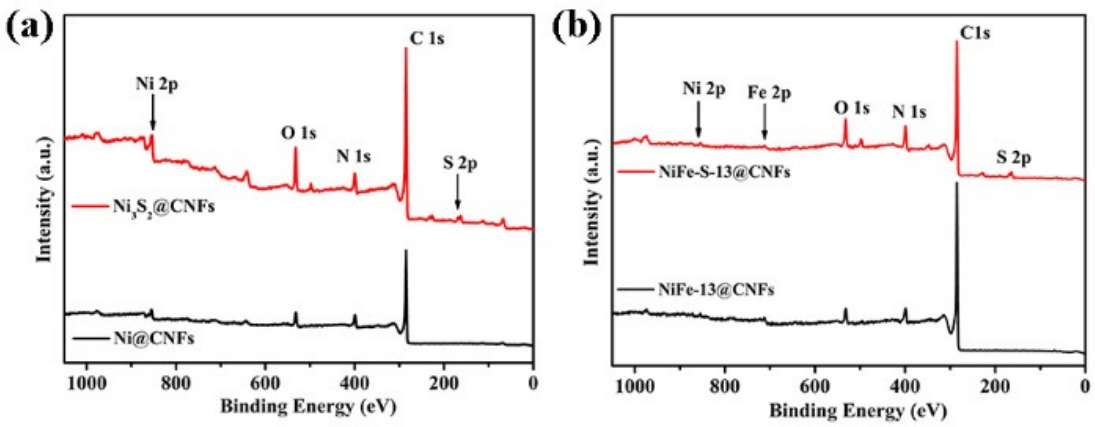

Fig. S6 (a) XPS surveys of Ni@CNFs and Ni_3S_2@CNFs; (b) XPS surveys of NiFe-13@CNFs and NiFe-S-13@CNFs.

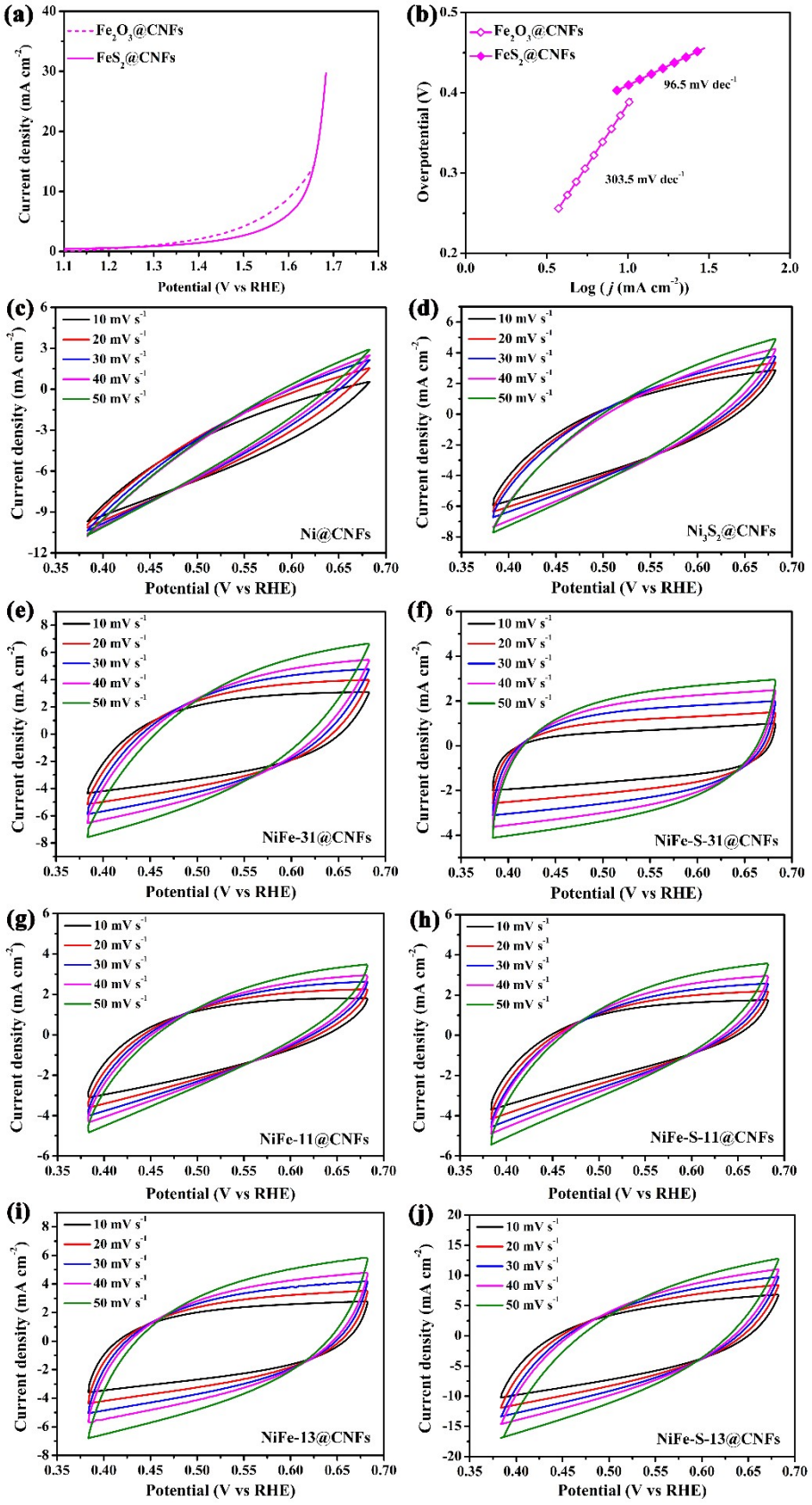
(a)
Fe2O3@CNFs
FeS2@CNFs
Current density (mA cm-2)
Potential (V vs RHE)
(b)
Fe2O3@CNFs
FeS2@CNFs
96.5 mV dec-1
303.5 mV dec-1
Overpotential (V)
Log (j (mA cm-2))
(c)
10 mV s-1
20 mV s-1
30 mV s-1
40 mV s-1
50 mV s-1
Ni@CNFs
Current density (mA cm-2)
Potential (V vs RHE)
(d)
Ni3S2@CNFs
(e)
NiFe-31@CNFs
(f)
NiFe-S-31@CNFs
(g)
NiFe-11@CNFs
(h)
NiFe-S-11@CNFs
(i)
NiFe-13@CNFs
(j)
NiFe-S-13@CNFs

Fig. S7 (a) LSV curves (iR-corrected) curves and (b) corresponding Tafel slope curves of of Fe_2O_3@CNFs and FeS_2@CNFs for OER in 1.0 M KOH, the required overpotentials were 385 and 408 mV at 10 mA cm^{-2} for Fe_2O_3@CNFs and FeS_2@CNFs, respectively; (c-j) Cyclic voltammetry curves at 0.38~0.68 V vs RHE with different scan rates from 10 to 50 mV s^{-1} for all samples.

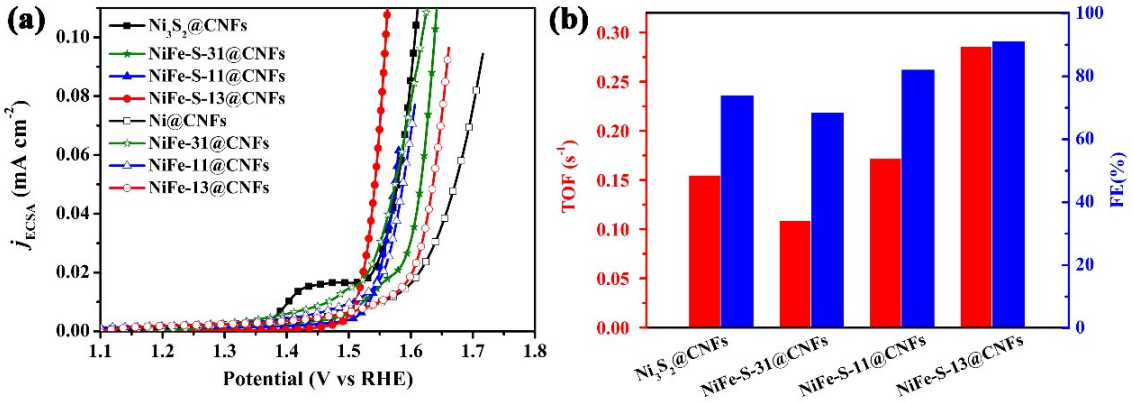

Fig. S8 (a) OER polarization curves standardized by ECSA for all-samples; (b) TOF values of at the overpotential of 300 mV and Faradic efficiency (FE) for Ni_3S_2@CNFs and NiFe-S@CNFs series.

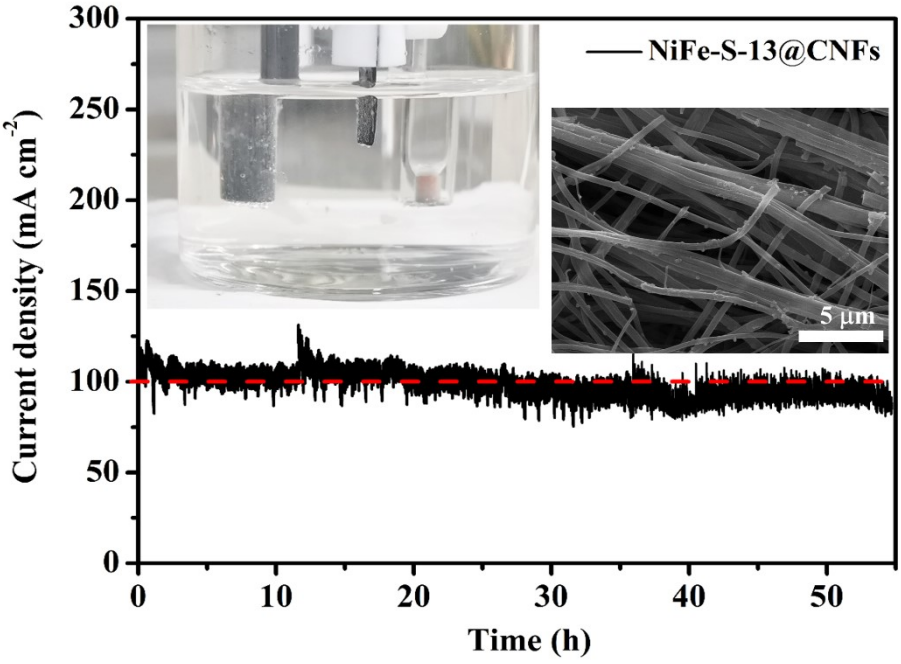

Fig. S9 Chronopotentiometry curve of NiFe-S-13@CNFs at high current density of 100 mA cm^{-2} for 55 h (inset: SEM image of NiFe-S-13@CNFs after durability and a photography of OER process).

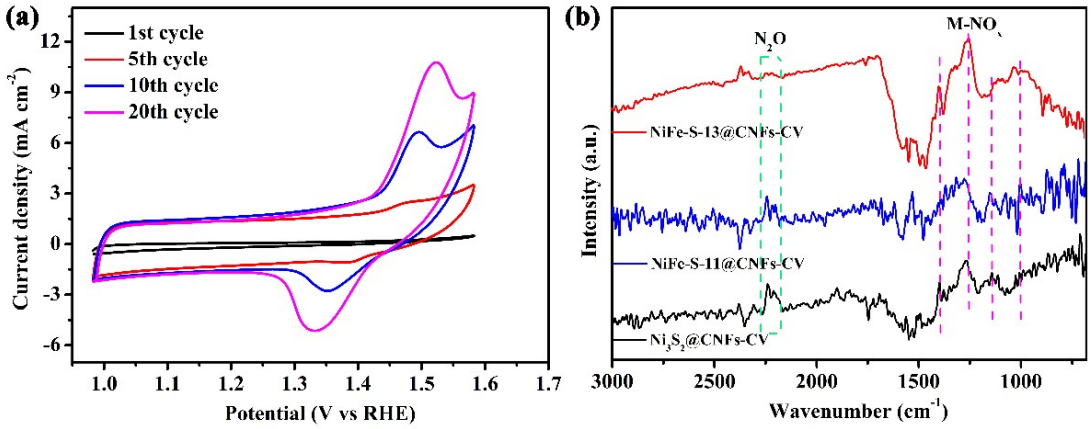

Fig. S10 (a) Cyclic voltammogram curves of Ni_3S_2@CNFs at different cycles; (b) *In situ* DRIFT spectra of NO adsorption for Ni_3S_2@CNFs, NiFe-S-11@CNFs and NiFe-S-13@CNFs after CV activation.

Fig. S10b presents that the peaks at 2209 and 2239 cm^{-1} are ascribed to the N_2O, indicated of the occurrence of partial NO reduction into N_2O. Meanwhile, the peaks around 1001-1398 cm^{-1} correspond to M-NO_x that are reaction intermediates NO_x species adsorbed on the metal sites. Compared to the Fe-free Ni_3S_2@CNFs, with the increasing Fe contents, the N_2O peak decreases while the M-NO_x peaks increase, implying that Fe site is mainly NO absorption site and the high oxidized Fe is formed.

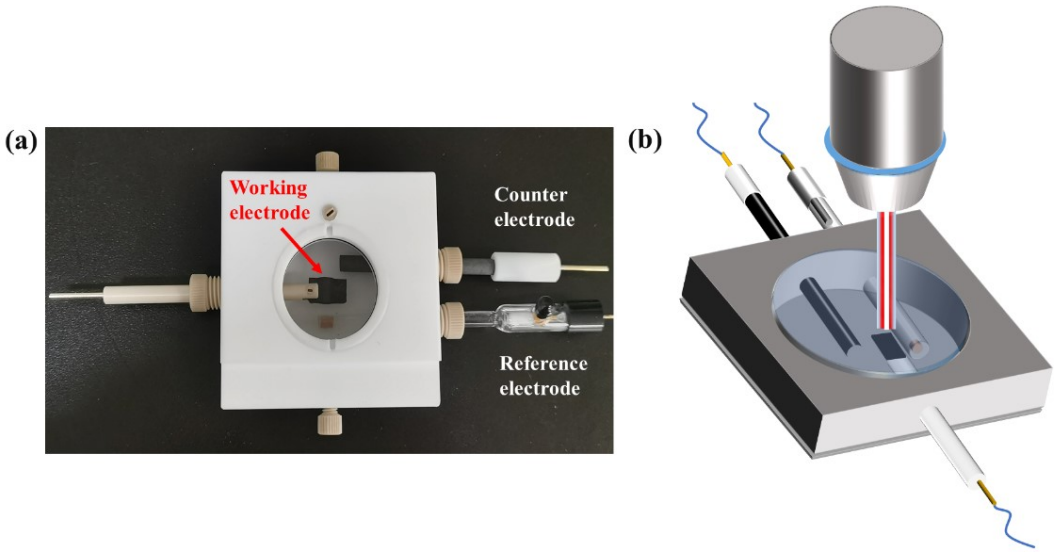

Fig. S11 (a) A photograph of *in-situ* Raman electrolysis cell. (b) Schematic illustration of *in-situ* Raman process.

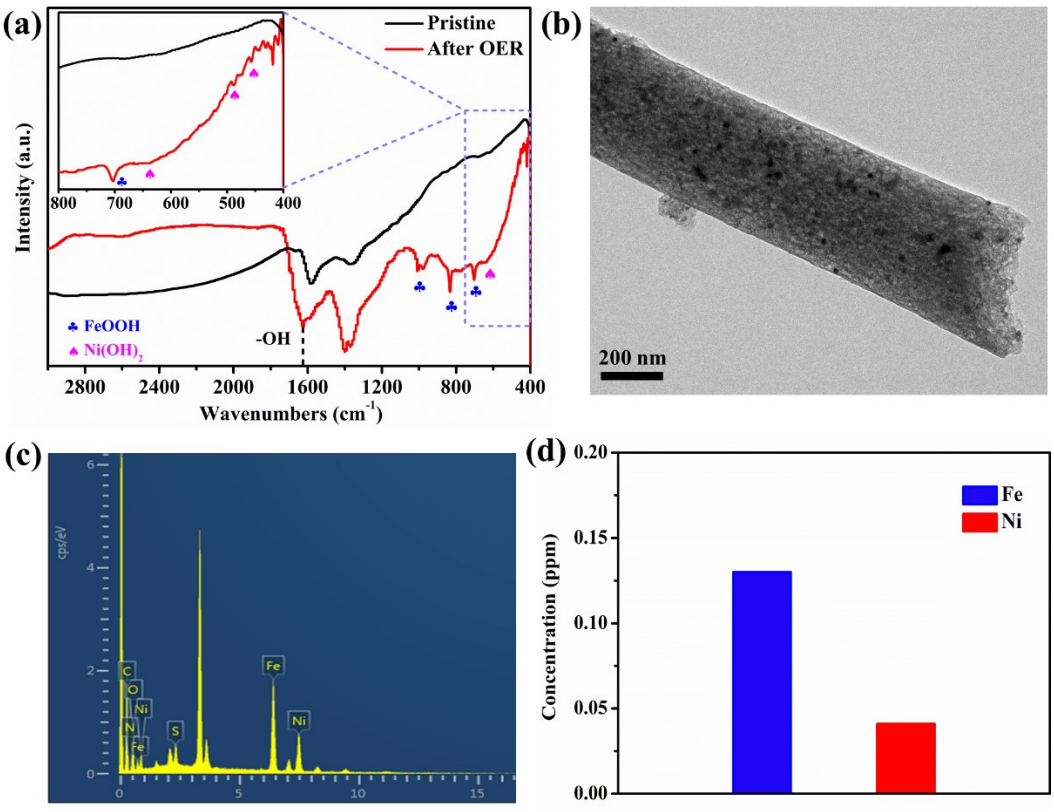

Fig. S12 (a) FTIR spectra, (b) TEM image and (c) EDS spectra of NiFe-S-13@CNFs after OER; (d) Concentration of Fe and Ni elements in electrolyte after durability of NiFe-S-13@CNFs.

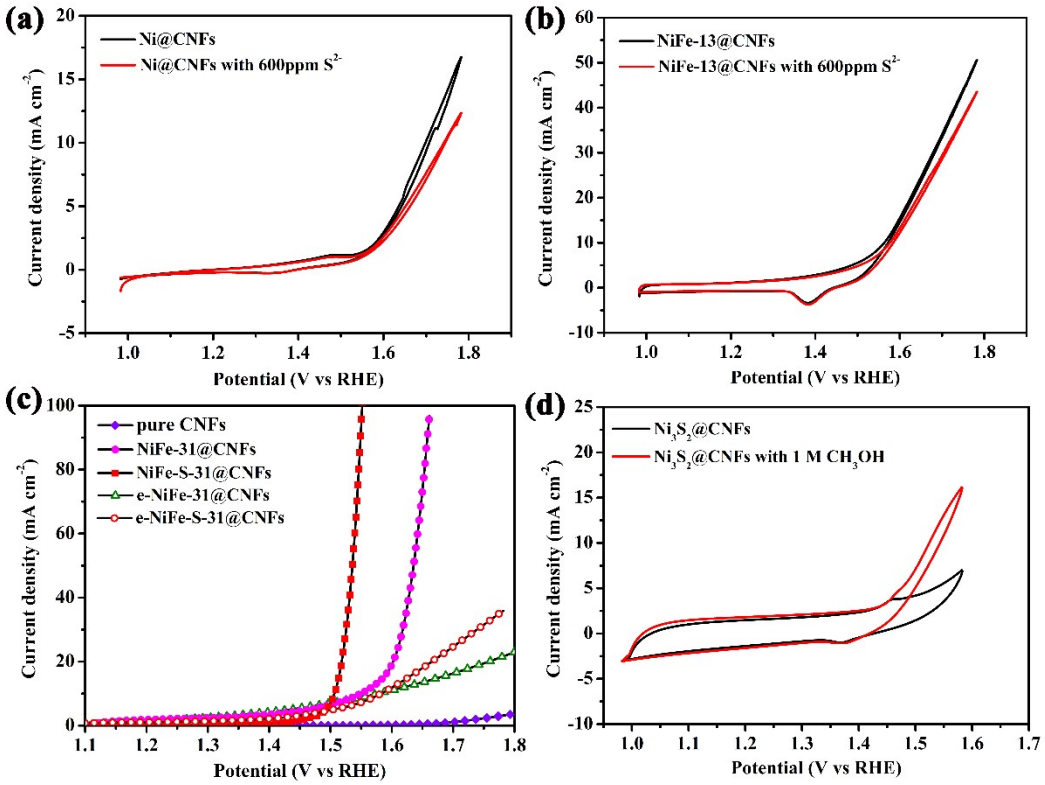

Fig. S13 CV curves of (a) Ni@CNFs and (b) NiFe-13@CNFs with and without 600 ppm S^{2-} in the electrolyte. (c) LSV curves (iR-corrected) for OER before and after oxalic acid treatment (PAN was carbonized to gain pure-CNFs without metals; e- NiFe-13@CNFs was prepared from acid treatment of NiFe-13@CNFs via using 0.5 M oxalic acid for 3 days; e-NiFe-13@CNFs was further sulfide to synthesize e-NiFe-S-13@CNFs). (d) CV curves (without iR-correction) of Ni_3S_2@CNFs before and after adding 1.0 M CH_3OH.

Table S1 Summary of fitted R_s, R_{ct} and C_{dl} values for all synthesized samples.

Samples	R_s / Ω	R_{ct} / Ω	C_{dl} / mF cm^{-2}
Ni@CNFs	11.85	6.55	8.19
NiFe-31@CNFs	9.47	2.89	4.27
NiFe-11@CNFs	9.89	1.977	28.9
NiFe-13@CNFs	9.16	0.24	40.1
Ni_3S_2@CNFs	7.62	0.35	9.2
NiFe-S-31@CNFs	8.63	0.61	15.8
NiFe-S-11@CNFs	5.38	0.49	39.8
NiFe-S-13@CNFs	4.66	0.19	53.7

Table S2 Properties comparison of recent reported electrocatalysts for OER.

Catalyst	Overpotential at 10 mA cm^{-2} (mV)	Tafel slope (mV dec^{-1})	Testing substrate	Ref
NiFe-S-13@CNFs	270	44.4	No-substrate	This work
(NiFe)S_2-GN-0.2	320	61	GCE[a]	3
(NiFe)S_2	262	56.2	GCE	4
Ni-Fe-OH@ Ni_3S_2	165	93	Nickel foam	5
Fe_{30}SPyr	284	39	Nickel foam	6
(Fe, Ni, Co)$_9S_8$@CS	260	45	GCE	7
Co_9S_8/CS-800	370	98	GCE	8
Ni-MoS_2/NC	261	53	RDE[b]	9
WS_2/Co_xS_y@N, S-co doped carbon	365	53	RDE	10
N-doped Ni-Ni_3S_2@carbon	284.7	61	GCE	11
CoMoS-600	350	64.32	GCE	12
Fe-CoS_2/CoS_2@NC	300	72	Carbon paper	13
Co@NC@MoS_2	297	70	GCE	14

a. GCE: glassy carbon electrode; b. RDE: rotating disk electrode

Reference:

1. C. C. L. McCrory, S. Jung, J. C. Peters and T. F. Jaramillo, *J. Am. Chem. Soc.*, 2013, **135**, 16977-16987.
2. M. Yan, Z. Zhao, P. Cui, K. Mao, C. Chen, X. Wang, Q. Wu, H. Yang, L. Yang and Z. Hu, *Nano Res.*, 2021, **14**, 4220-4226.
3. C. Liu, H. Ma, M. Yuan, Z. Yu, J. Li, K. Shi, Z. Liang, Y. Yang, T. Zhu, G. Sun, H. Li and S. Ma, *Electrochim. Acta*, 2018, **286**, 195-204.
4. B. Ni, T. He, J. O. Wang, S. Zhang, C. Ouyang, Y. Long, J. Zhuang and X. Wang, *Chem Sci*, 2018, **9**, 2762-2767.
5. X. Zou, Y. Liu, G. D. Li, Y. Wu, D. P. Liu, W. Li, H. W. Li, D. Wang, Y. Zhang and X. Zou, *Adv Mater*, 2017, **29**.
6. J. Tzadikov, R. Geva, A. Azoulay and M. Shalom, *ChemCatChem*, 2021, **13**, 3749-3753.
7. Y. Kim, M. Karuppannan, D. Lee, H. E. Bae, Q. T. Luong, S. Y. Kang, Y.-E. Sung, Y.-H. Cho and O. J. Kwon, *Int. J. of Energ. Res.*, 2022, **46**, 3145-3154.
8. W. Li, Y. Li, H. Wang, Y. Cao, H. Yu and F. Peng, *Electrochim. Acta*, 2018, **265**, 32-40.
9. J. Jiang, J. Chen, P. Jiang, Y. Leng and W. Jin, *ChemCatChem*, 2019, **11**, 1185-1191.
10. Z. Huang, Z. Yang, M. Z. Hussain, B. Chen, Q. Jia, Y. Zhu and Y. Xia, *Electrochim. Acta*, 2020, **330**, 135335.
11. Y. Lin, G. Chen, H. Wan, F. Chen, X. Liu and R. Ma, *Small*, 2019, **15**, 1900348.
12. Z. Huang, Z. Yang, Q. Jia, N. Wang, Y. Zhu and Y. Xia, *Nanoscale*, 2022, **14**, 4726-4739.
13. C. Yang, Y.-X. Chang, H. Kang, Y. Li, M. Yan and S. Xu, *App. Phys. A*, 2021, **127**, 465.
14. A. Gaur, P. K. Sachdeva, R. Kumar, T. Maruyama, C. Bera and V. Bagchi, *Sustain. Energ. Fuels*, 2021, **5**, 801-807.